**Role of Si/Al Ratio on Immobilization and Stability of Rhodium Complexes on ZSM-5**

By

Brandon Long

Submitted to the graduate degree program in Chemical and Petroleum Engineering and the Graduate Faculty of the University of Kansas in partial fulfillment of the requirements for the degree of Master of Science.

_____
Dr. Javier Guzman (Chair)

_____
Dr. Aaron Scurto

_____
Dr. Susan Stagg-Williams

Date defended: _____

The Thesis Committee for Brandon Long certifies that this is the approved Version of the following thesis:

**Role of Si/Al Ratio on Immobilization and Stability of Rhodium Complexes on ZSM-5**

_____
Dr. Javier Guzman (Chair)

_____
Dr. Aaron Scurto

_____
Dr. Susan Stagg-Williams

Date approved: _____

**Table of Contents**

**List of Figures**

**List of Tables**

**Abstract**

Rhodium complexes within the pores of zeolite ZSM-5 with varying Si/Al ratios (Si/Al 23, Si/Al 50, and Si/Al 280) were prepared from $Rh^{1+}(CO)_2(C_5H_7O_2)$, $Rh_2^{2+}(CO_2CH_3)_4$, and $Rh^{3+}(C_5H_7O_2)_3$ followed by thermal treatment in He. IR results indicate that changing the Si/Al ratio stabilizes different Rh species, with the formation of Rh(I), Rh(II), or Rh(III) complexes along with the ability to coordinate two to four ligands. Through X-ray absorption spectroscopy, changes in oxidation state are followed and the final structure determined. Both the Si/Al ratio and rhodium precursor structure play a role, with Rh clusters of two atoms, four atoms, or six atoms immobilized on ZSM-5. Differences in bond lengths are affected by Si/Al ratio, creating tighter or more expanded clusters. This variation in structure caused by the Si/Al ratio shows potential for affecting the amount of hydrogen produced from the partial oxidation of methanol.

**Acknowledgements**

I would like to thank Dr. Javier Guzman for guidance, ideas, and support while working on this research. The graduate and undergraduate members of the research group also provided valuable support and help in finishing up lab work. I thank CEBC for exposing me to new topics of importance in the environmental area, and for the funding of all research. Finally, I am sincerely grateful to my fellow grad students, namely Mark and Madhav, who helped through the years with their support and friendship.

# Chapter 1: Introduction

## 1.1 Overview

The idea of having uniform, single-sites is a growing area in catalysis research. Traditionally, this terminology could not be applied to heterogeneous catalysis, as it is typical to create catalysts with a wide spectrum of sites with differing structure and reaction parameters. For homogeneous catalysts, however, similar active sites are the norm, and in fact it is a given that all sites are the same. With the catalyst in solution, there is no additional anchoring needed, which tends to distort the arrangement and behavior of the initial metal centers. Therefore, research is conducted to create heterogeneous catalysts which would share similar properties as their homogeneous brethren.

With this in mind, a new area of heterogeneous catalysis is emerging which focuses on controlling the active centers at the atomic scale where the reaction takes place, which is the emphasis for this research. The primary attribute of these so-called single-site catalysts is the ability to create a catalyst with a uniform distribution of known active sites. If the structural characteristics of the catalyst are known and can be controlled, along with the resulting effect on its participation in catalysis, then optimization of catalysts can be achieved to increase reaction rates.

One such method for creating defined catalysts exploits zeolites which have specific sites for anchoring metals. This project will use the zeolite ZSM-5 as a support, and the active center for the catalyst will be the transition metal rhodium. There is current literature which studies the anchoring of rhodium inside zeolite cages, and part of the aim of this research is also to expand the knowledge base of this particular area.

Characterization techniques will be utilized to investigate the stability and anchoring of rhodium sites within zeolite pores. The first is infrared spectroscopy (FTIR) during CO adsorption. This method is used to elucidate the oxidation and coordination of the resulting rhodium species. Secondly, X-ray absorption spectroscopy (XAS) will further expand on these results through two complementary techniques: X-ray absorption near edge spectroscopy (XANES) and extended X-ray absorption fine structure (EXAFS). XANES allows one to track changes in oxidation state and from EXAFS the species present around the metal center can be determined, ultimately leading to the coordination and arrangement within the support. Finally, the production of hydrogen from methanol via partial oxidation will be investigated to determine effects on the reaction due to changes in the catalyst.

### 1.2 Zeolite ZSM-5

Zeolites are aluminosilicates which possess a very regular microporous structure; because of this consistency, small channels exist through which chemicals can flow.

Within zeolites, ZSM-5 is a synthesized zeolite which has pore diameters of about 5.5 Å. Figure 1.1 shows the ZSM-5 structure.

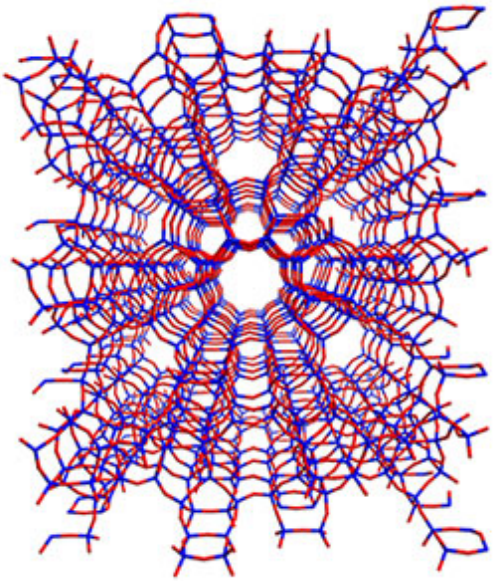

**Figure 1.1. Picture of ZSM-5 structure.**[1]

The fascinating aspect of zeolites is the ability to exchange the framework atoms. For ZSM-5 it is common to replace $Si^{4+}$ with $Al^{3+}$, thereby creating a positive charge which is compensated with $H^{+}$, creating Bronsted acid sites.[1] The ratio of silicon to aluminum atoms can by varied, ranging from Si/Al 23 up to Si/Al 280. Acid-catalyzed reactions can proceed with ZSM-5 as is, using these Bronsted sites for reaction.[2] The zeolite can be further manipulated, however, by replacing the protons with metals, and thus the ability to create numerous catalysts is born. Though these are not necessarily Bronsted acid sites after the proton has been exchanged for the metal, it is still common to refer to the acidity of zeolites when distinguishing

between zeolites of differing aluminum content. Catalysts are then created with high acidity, Si/Al 23, or very low acidity, Si/Al 280, and variances in between as the number of cationic sites changes. For this study, ZSM-5 with Si/Al ratios of 23, 50, and 280 are used. By changing the acidity of the zeolite, in essence the proximity of cationic sites is also being changed so that sites are closer or farther apart from each other. For Si/Al 23, there are 1-2 cationic sites available per unit cell, for Si/Al 50 less than 1 site per unit cell is available, and Si/Al 280 has very few. The dimensions of a unit cell for ZSM-5 are 20 Å x 20 Å x 13 Å. Also, since zeolites have a regular pore structure, when the acid sites are created each one is the same in regard to the atoms and environment surround it, thus giving the unique opportunity to create uniform, single-site catalysts.

### 1.3 Single-Site Heterogeneous Catalysis

Within heterogeneous catalysts, the different types of single-site catalysts are categorized into four broad groups, with a summary of the main points to follow.

The first category includes individual ions, atoms, or molecular complexes anchored to high-area supports such as silica. Maschmeyer presents a titanium catalyst used for epoxidation where $Ti^{4+}$ centers are grafted to three oxygens of the silica support, which is very stable and resistant to leaching.[3] Also, the $Ti^{4+}$ centers are separated by at least 7 Å, since the starting titanium precursor includes large ligand groups, but

which do not appear in the final catalytic form. Similar grafting techniques are utilized to isolate $Mo^{6+}$ and $Cr^{6+}$.[4, 5] Large organometallic complexes are also capable of producing individual active sites, as shown by both Basset and Marks. Basset and coworkers show work involving Mo and Re complexes, each with three large organic ligands supported on the surface of nonporous silica for use in metathesis reactions.[6] While Marks and coworkers start with a homogeneous metallocene catalyst, and are able to anchor it onto either alumina or zirconia supports; they have studied complexes of Zr, Th, and Ti and has shown promising results for each.[7-9]

The binding of organometallic species to mesoporous silica supports are also able to yield single-site catalysts. This second category is similar to the previous section, but involves tethering of the complexes to the inner walls of the support. Through the synthesis technique, the outer walls of the mesoporous support are neutral, while inside the pore a variety of functionalized complexes can be attached to propyl bromide, which is bonded to the pore wall.[10]

The third area of single-site heterogeneous catalysts is dubbed ship-in-bottle catalysts; molecular complexes are entrapped within zeolitic cages that are permeable only to certain reactants and products. Examples include encapsulating cis-$[Mn(bipyridine)_2]^{2+}$ within zeolite Y pores for the epoxidation of alkenes,[11] and colbalt Salophen within a zeolite useful in the oxidation of alcohols.[12]

This research project falls under the fourth category discussed, which uses microporous supports, typically zeolites, and creates active sites located near ions which replace framework ions of the original support. For zeolites, the framework structure is $SiO_4$, and Si can be replaced with other atoms such as Al. When anchoring metals inside the zeolite pores around the Al, two types of centers are commonly seen: either a monatomic metal site or a small cluster of metal atoms. A brief example showing each of these active centers follows.

Monatomic sites using the metals rhenium and rhodium are supported in the pores of zeolite Y. An example of rhodium includes a project focused on identifying the structure, using EXAFS in conjunction with density functional theory.[13] No treatment on the catalyst is used; rather, they anchor the metal at room temperature and evaluate what is present. The research concludes that one Rh bonds inside the zeolite pore, and is oriented around the Al atom. The Rh does not bond directly to the aluminum, but rather to the two oxygens on either side. A similar study using rhenium explores the catalytic site using a test reaction.[14] The rhenium precursor starts with ethylene ligands already present, and looks at hydrogenation of ethylene with $H_2$. Knowing that ethylene will react readily with the rhenium atom, the research explores the stability of the mononuclear atom and its ligands. Using in-situ IR and EXAFS to follow the reaction, changes to the rhenium structure are seen under operating conditions. Initially the mononuclear Re is coordinated to the zeolite

via three framework oxygens around the Al, and has three ethylene ligands. When the reaction occurs, however, bonds to the ligands and framework are lost, such that either two or three sites are then available take part in the reaction. The Re itself though still stays as a single atom.

In addition, investigations have additionally shown the ability to form active sites of small four or six atom Ir and Rh clusters. Similar to above, IR and EXAFS are utilized to follow the structure of Ir and Rh within zeolite pores as the stability of each is tested with multiple gas treatments.[15, 16] Each catalyst is treated under CO flow at 125 °C, whereupon they report the formation of clusters, $Ir_4(CO)_{12}$ and $Rh_6(CO)_{16}$. Decarbonylation follows this, treating each catalyst at 300 °C with He, and then recarbonylation again. Structural investigations after each of these two treatments shows the same results as initially, with small four or six atom clusters present; the active site is indeed stable within the pore and does not agglomerate. This is compared to Ir clusters formed on the surface of the zeolite, where although initially four iridium atoms are joined, upon decarbonylating in He, there are now agglomerates of approximately 20 iridium atoms. Thus, bonding of the metal atoms around Al within the zeolite pore is key and does prove to be a stable process.

## 1.4 Methanol to Hydrogen

Alternatives for energy production are currently being researched as a way to move away from fuels which are commonly dirty, such as oil or coal, which emit a number of pollutants such as VOC's, $NO_x$, $SO_x$, and particulate matter. They contribute to the ozone layer and can cause respiratory problems amongst other health issues. One such alternative energy source is hydrogen; specifically, hydrogen production from methanol for use in Proton Exchange Membrane (PEM) fuel cells. Hydrogen has the highest energy density of any non-nuclear fuel, and can be produced and used on-board.[17] Methanol reforming is an ideal candidate as it is essentially a clean technology with only limited amounts of $CO_2$ in the reaction, and the absence of carbon–carbon bonds reduces the risk of coke formation.[18] The fact that it is sulfur free eliminates any concerns about poisoning of the catalyst in the fuel cell. Moderate reaction temperatures are also possible; in the range of 200–300 $^{o}$C is typical. Currently, about 90% of methanol is produced from natural gas, through the production of synthesis gas and its subsequent conversion to methanol. In addition to natural gas, methanol can be produced from other gasification routes such as coal and biomass.

For hydrogen production from methanol there are two main reactions: the partial oxidation of methanol (Eqn. 1) and methanol steam reforming (Eqn. 2).[19]

$$CH_3OH + \tfrac{1}{2}O_2 \rightarrow CO_2 + 2H_2 \quad \left(\Delta H^o = -154.8 kJ/mol\right) \qquad (1)$$

$$CH_3OH + H_2O \rightarrow CO_2 + 3H_2 \quad \left(\Delta H^o = +131 kJ/mol\right) \qquad (2)$$

$$CH_3OH + \tfrac{1}{2}H_2O + \tfrac{1}{4}O_2 \rightarrow CO_2 + \tfrac{5}{2}H_2 \quad \left(\Delta H^o = -12 kJ/mol\right) \qquad (3)$$

As can be seen, the partial oxidation of methanol is a highly exothermic process while steam reforming is endothermic. Heat transfer distribution within the catalyst plays a major role in catalyst design and the commercialization of the technology. However, in oxidative methanol steam reforming (Eqn. 3) the reactions combine to yield a process which is only slightly exothermic and in fact has close to negligible heat effects. From a hydrogen production standpoint, steam reforming has the best $H_2$:$CO_2$ ratio, 3:1, and is thus very efficient in converting the methanol into a usable energy source. With each route the production of CO is a major factor as it must be kept to low levels or it will deactivate the Pt electro-catalysts used in current PEM fuel cells.[20] This research focuses solely on the partial oxidation of methanol, using pure $O_2$ as the oxidant. This is done so the relationship to other oxidation reactions could be easier to propose, after the results of the effect of Si/Al ratio are known.

To produce hydrogen, research groups are mainly focusing on the use of Cu, Zn, and Pd metals on oxide supports for the catalyst. One such study looks at related work, as Cu and Zn are immobilized on the zeolite ZSM-5 to investigate how the different

characteristics of zeolites influence activity.[21] Catalysts are prepared either with copper or incorporating both copper and zinc. For the study indicated, only the methanol steam reforming reaction is looked at, so no $O_2$ is added. At a temperature of 250 °C, 95% of the methanol is converted with a hydrogen yield of 64% for the combined catalyst while copper alone gives 89% methanol conversion and only 38% hydrogen yield. Also of note, the Cu/Zn catalyst will yield 82% hydrogen at 275 $^{o}$C; there is clearly a promoter effect with zinc. Different Si/Al ratios are also tested, with lower ratios giving better conversion and yield. This is synonymous with saying that the more acidic zeolite has higher activity for methanol steam reforming. Comparisons were also made against a BASF catalyst using the standard $Cu/Zn/Al_2O_3$; the alumina supported catalyst shows higher activity than the zeolite catalyst. Trends for alumina versus zeolite supports are shown in Figure 1.2; the zeolite supports show respectable results, but there is still room for improvement.

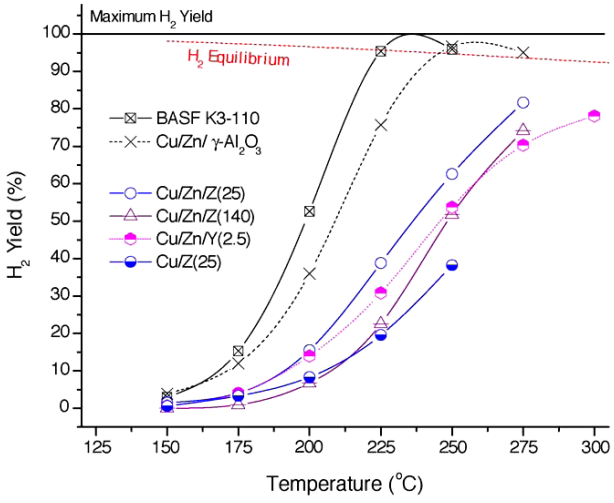


**Figure 1.2. Hydrogen yields of methanol steam reforming over selected zeolite catalysts.**[21]

## 1.5 X-ray Absorption Spectroscopy Theory

For part of this research project, a spectroscopic technique will be utilized which is becoming much more prominent in identifying and characterizing catalysts.[22] X-ray absorption spectroscopy (XAS) has grown with the advent of large-scale synchrotrons, which provide a consistent and powerful photon supply.[23] The basic idea of XAS involves bombarding a sample with photons of a certain energy, which eject electrons.[24] The energy corresponds to the binding energies of the 1s (k-edge) or 2s and 2p orbitals ($L_I$, $L_{II}$, and $L_{III}$ edges) of a specific metal in the sample. As the electrons are ejected they emanate from the atom in what is described as a wave-like pattern (Figure 1.3). The waves of electrons radiate outward, coming in contact with nearby atoms, which interfere with the pattern causing the wave to bounce back towards the initial atom (backscattering). Backscattering is affected by the type of atom contacted along with its distance away, so the wave is very different depending on the exact nature of the atom. What we then have are waves of electrons going out from the metal atom (dashed lines in Figure 1.3), some of the electrons reversing course through backscattering (solid lines in Figure 1.3), and the outgoing and incoming waves interacting with each other as they cross paths.

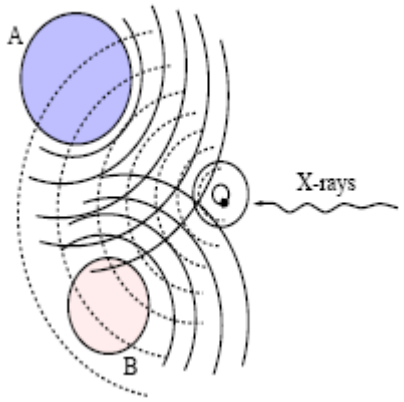


**Figure 1.3. A cartoon showing the basic idea of how XAS works.[25] A and B represent atoms nearby the main metal atom.**

The XAS detectors measure the absorption coefficient which is affected by the interference of the electrons, resulting in a plot of absorption coefficient versus energy. The energy range starts 100 eV below the binding energy (or edge) and extends to 1000 eV above the binding energy. The XAS data is broken into two regions for analysis; X-ray absorption near edge spectroscopy (XANES) and extended X-ray absorption fine structure (EXAFS). XANES looks at a small region right around the edge, from -30 eV to +50 eV. At the edge a large jump in the absorption coefficient is seen resulting in a peak; the peak height and position are commonly associated with the oxidative environment around the metal atom, so changes to it are monitored. EXAFS looks at the whole energy range and is able to give the types of atoms nearby, the number of atoms, and bonding distance. EXAFS analysis is much more complex, and involves taking the absorption coefficient data and plugging it into a number of equations to convert the data into chi ($\chi$) and Fourier

Transform (FT) plots. Software (XDAP) is available which does these calculations. With the data now in its chi and FT form, using XDAP, a model is fit to the data until a sufficient fit is achieved, and the result is the surrounding atomic structure.

## 1.6 Research Objectives

Zeolite supports pose an intriguing option for catalysis through their ability to be tuned to meet specific standards. Most notably, changing the Si/Al ratio is being studied to determine its full effect on the anchoring of metals and the subsequent reaction characteristics. There are reports which show that having lower Si/Al ratios leads to increases in reaction rate; however, none of the groups pose reasons as to what exactly changed to cause this.[26, 27]

This idea is further studied for Rh-ZSM-5 systems; investigating the effect of Si/Al ratio by using zeolite supports with Si/Al ratios of 23, 50, and 280. Furthermore, when synthesizing the catalysts three rhodium precursors are used with increasing oxidation states to see how the results compare; the precursors are $Rh^{1+}(CO)_2(C_5H_7O_2)$, $Rh_2^{2+}(CO_2CH_3)_4$, and $Rh^{3+}(C_5H_7O_2)_3$. Table 1.1 gives the notation procedure to be used throughout this thesis for each of the nine catalysts. In addition to differences in oxidation state, each of the precursors also have very unique structures which could affect the final state of the active center. The synthesized catalysts will undergo a series of tests to characterize the nature of the rhodium center

to see if distinguishable differences are present. IR and XAS spectroscopies will be drawn upon to perform these studies, giving the coordination and oxidation of the rhodium within the zeolite pore. With the results from the spectroscopies in hand, the partial oxidation of methanol to produce hydrogen will be used as a test reaction to see how the changes in catalyst composition influence the reactivity.

As a note, only IR data is available for catalysts synthesized using $Rh^{3+}( C_5H_7O_2)_3$.

**Table 1.1. Nomenclature to be used to distinguish between catalysts.**

| | ZSM-5 Si/Al Ratio | | |
|---|---|---|---|
| Rhodium precursor | 23 | 50 | 280 |
| $Rh^{1+}(CO)_2(C_5H_7O_2)$ | Si/Al 23:Rh(I) | Si/Al 50:Rh(I) | Si/Al 280:Rh(I) |
| $Rh_2^{2+}(CO_2CH_3)_4$ | Si/Al 23:Rh(II) | Si/Al 50:Rh(II) | Si/Al 280:Rh(II) |
| $Rh^{3+}( C_5H_7O_2)_3$ | Si/Al 23:Rh(III) | Si/Al 50:Rh(III) | Si/Al 280:Rh(III) |

## Chapter 2: IR Spectroscopy – CO Adsorption Studies

### 2.1 Abstract

The effect of zeolite ZSM-5 Si/Al ratio on adsorption of CO to rhodium is investigated using three different rhodium precursors. Typical dicarbonyl ligands ($Rh^{1+}(CO)_2$) are present in all cases, but tricarbonyl and tetracarbonyl ligands on Rh(I) are also stable in catalysts with Si/Al ratios of 23 and 50. Also, the ability to form rhodium species with oxidation states of $2^+$ or $3^+$ (Rh(II)-CO and Rh(III)-CO) is shown in Si/Al 23 and 50 catalysts. In both cases, Si/Al 23 catalysts have greater stability of these unique species, as their peak intensities are greater than those of Si/Al 50 catalysts. None of the catalysts with Si/Al of 280 are able to stabilize species other than the $Rh^{1+}(CO)_2$. This further shows the effect of changing the Si/Al ratio within catalysts to alter the types and stability of bonds present within zeolite pores.

### 2.2 Introduction

For zeolite catalysts, Bronsted acidity can be manipulated by exchanging $Si^{4+}$ for $Al^{3+}$ ions. At higher exchange rates, increased local acidity affects the bonding of metal cations within the zeolite pore structure. This idea is further studied for rhodium anchored on ZSM-5, investigating the effect of Si/Al ratio by synthesizing catalysts

with Si/Al ratios of 23, 50, and 280. It is well established that using CO as a probe molecule coupled with Infrared spectroscopy can give valuable information.[28-30] For rhodium catalysts, the adsorption of carbonyl ligands will give rise to IR frequencies which can be specifically linked to the coordination and oxidation state of the resulting complex. Comparisons can then be made among the Si/Al ratios to determine what role the local acidity plays.

To perform this investigation, CO will be passed over the rhodium on ZSM-5 catalysts and followed via IR. As CO adsorbs onto the rhodium species, the resulting IR frequencies will be monitored and used to determine the structure.

## 2.3 Experimental

ZSM-5 zeolites with Si/Al ratios of 23, 50, and 280 were purchased from Zeolyst International and calcined at 400 °C for 2 hours in air. Either $Rh(CO)_2(acac)$, $Rh_2(CO_2CH_3)_4$, or $Rh(acac)_3$ (where acac is $C_5H_7O_2$) was combined with the calcined ZSM-5 zeolite in a Schlenk flask, with the mixture composition chosen so that the resultant solid contained 1 wt% Rh. Dried and deoxygenated toluene was introduced to the Schlenk flask and the slurry was stirred for 24 hours at room temperature. The solvent was then removed by evacuation over a 24 hour period, with a dry powder remaining. Each catalyst was treated in a tube furnace at 225 °C for 6 hours under He flow to bring the catalyst to its final state.

Experiments were performed using a Bruker Tensor 27 spectrometer, averaging 64 scans at a resolution of 4 $cm^{-1}$. Each catalyst was pressed into a wafer made with .015 g powder, using a hand press to form sufficiently thin samples. To perform flow studies, the wafer is placed into a High-Low Infrared Reactor purchased from In-Situ Research Instruments allowing for temperature and environment control. A cylinder of 10% CO in He (Airgas) was used for all CO flow studies, passing it through moisture and $O_2$ removal traps.

## 2.4 Results and Discussion

The most prominent feature in all plots are two peaks both assigned to dicarbonyls, $Rh^{1+}(CO)_2$. With frequencies of 2116 and 2049 $cm^{-1}$, they are the symmetric and antisymmetric vibrations of CO; in literature rhodium dicarbonyls are the most stable and prevalent species and so this is not unexpected.[30] There are no major differences between the catalysts of differing Si/Al ratio when looking at these dicarbonyl species. Subsequent discussion will focus on the stability of less populous species, which however give one the ability to further elucidate trends and characteristics of the bonding within zeolite pores. Figures 2.1, 2.2, and 2.3 show the IR data for each of the catalysts and are separated so each figure represents one of the three Rh precursors with two Si/Al ratios. A summary of the peaks which are stable after releasing CO are also given in table format: Table 2.1, Table 2.2, and Table 2.3.

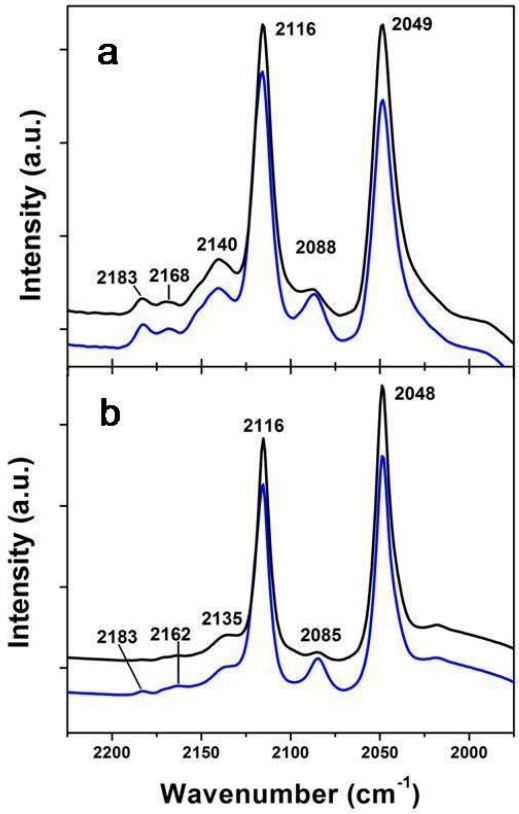


**Figure 2.1. FTIR plots of CO adsorption peaks for (a) Si/Al 23:Rh(I) and (b) Si/Al 50:Rh(I). Lines in blue are data taken under CO atmosphere and black lines are after CO release.**

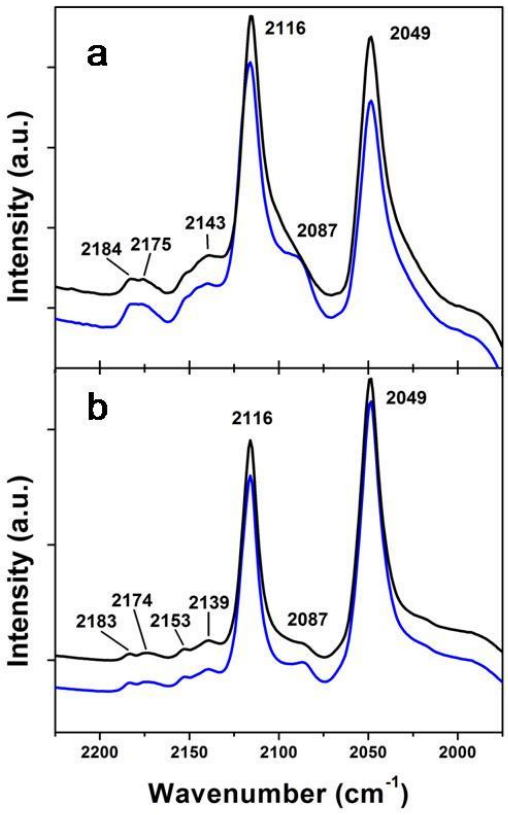


**Figure 2.2. FTIR plots of CO adsorption peaks for (a) Si/Al 23:Rh(II) and (b) Si/Al 50:Rh(II). Lines in blue are data taken under CO atmosphere and black lines are after CO release.**

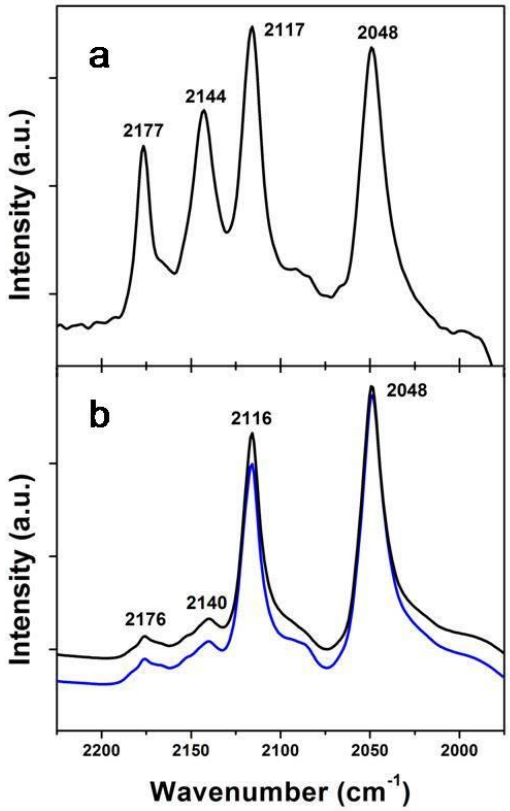


**Figure 2.3. FTIR plots of CO adsorption peaks for (a) Si/Al 23:Rh(III) and (b) Si/Al 50:Rh(III). Lines in blue are data taken under CO atmosphere and black lines are after CO release. For plot a, there was no difference after CO release so only one plot is shown.**

**Table 2.1. IR frequencies for CO adsorption on Rh(I) catalysts. Only those peaks which are still present after releasing CO are marked, since they are the stable species.**

| | | | Si/Al 23:Rh(I) | Si/Al 50:Rh(I) | Si/Al 280:Rh(I) |
|---|---|---|---|---|---|
| IR CO Peak Frequencies (cm-1) | $ZSM/Rh^{+}(CO)_2$ | 2049 | x | x | x |
| | | 2116 | x | x | x |
| | $ZSM/Rh^{+}(CO)_3$ | 2084 | x | x | |
| | | 2183 | x | | |
| | $ZSM/Rh^{+}(CO)_4$ | 2135 | | x | |
| | | 2162 | | | |
| | $ZSM/Rh^{2+}(CO)_2$ | 2142 | x | | |
| | | 2176 | | | |
| | $ZSM/Rh^{3+}CO$ | 2168 | x | | |

**Table 2.2. IR frequencies for CO adsorption on Rh(II) catalysts. Only those peaks which are still present after releasing CO are marked, since they are the stable species.**

| | | | Si/Al 23:Rh(II) | Si/Al 50:Rh(II) | Si/Al 280:Rh(II) |
|---|---|---|---|---|---|
| IR CO Peak Frequencies (cm-1) | $ZSM/Rh^{+}(CO)_2$ | 2049 | x | x | x |
| | | 2116 | x | x | x |
| | $ZSM/Rh^{+}(CO)_3$ | 2084 | | x | |
| | | 2183 | x | x | |
| | $ZSM/Rh^{+}(CO)_4$ | 2135 | | | |
| | | 2162 | | | |
| | $ZSM/Rh^{2+}(CO)_2$ | 2142 | x | x | |
| | | 2176 | x | x | |
| | $ZSM/Rh^{3+}CO$ | 2168 | | | |

**Table 2.3. IR frequencies for CO adsorption on Rh(III) catalysts. Only those peaks which are still present after releasing CO are marked, since they are the stable species.**

| | | | Si/Al 23:Rh(III) | Si/Al 50:Rh(III) | Si/Al 280:Rh(III) |
|---|---|---|---|---|---|
| IR CO Peak Frequencies (cm-1) | $ZSM/Rh^{+}(CO)_2$ | 2049 | x | x | x |
| | | 2116 | x | x | x |
| | $ZSM/Rh^{+}(CO)_3$ | 2084 | | | |
| | | 2183 | | | |
| | $ZSM/Rh^{+}(CO)_4$ | 2135 | | | |
| | | 2162 | | | |
| | $ZSM/Rh^{2+}(CO)_2$ | 2142 | x | x | |
| | | 2176 | x | x | |
| | $ZSM/Rh^{3+}CO$ | 2168 | | | |

Rhodium also possesses the ability to coordinate more ligands around it, but typically not under normal conditions; here data is presented which shows the stability of tricarbonyl and tetracarbonyl ligands. Tricarbonyl peaks arising from $Rh^{1+}(CO)_3$ have frequencies of 2085-2088 and 2183-2184 $cm^{-1}$.[28, 30] A rare tetracarbonyl species due to $Rh^{1+}(CO)_4$ has frequencies of 2135 and 2162 $cm^{-1}$.[28] Of the tricarbonyl peaks, the 2085-2088 $cm^{-1}$ frequency is known to appear under CO atmosphere, but then diminishes as CO is released. This phenomenon is seen in our data; however, in certain catalysts the tricarbonyl peak is still present after purging the cell with He. The catalysts showing this ability are Si/Al 23:Rh(I), Si/Al 50:Rh(I), and Si/Al 50:Rh(II). The 2183-2184 $cm^{-1}$ tricarbonyl peak also shows differences due to changing the Si/Al ratio. The Si/Al 23:Rh(I), Si/Al 50:Rh(I), Si/Al 23:Rh(II), and Si/Al 50:Rh(II) catalysts have this peak under CO atmosphere, with all but the Si/Al 50:Rh(I) catalyst showing stability after CO releases. The Si/Al

50:Rh(I) catalyst has frequencies associated with $Rh^{1+}(CO)_4$; they are however extremely small with only the 2135 $cm^{-1}$ peak still visible after releasing CO.

The presence of tricarbonyl or tetracarbonyl species without CO gas flowing shows a unique property, with the Si/Al ratio playing a role in this stabilization. For the rhodium precursors starting with Rh(I) and Rh(II), the relative peak intensities are greater for Si/Al 23 than for Si/Al 50, and Si/Al 280 shows no stability towards more CO ligands. The catalyst using the Rh(III) precursor does not coordinate more than the dicarbonyl ligands on any Si/Al ratio. For CO bonding and the formation of $Rh^{1+}(CO)_3$ and $Rh^{1+}(CO)_4$ species, lowering the Si/Al ratio has a positive effect on stability.

In addition, the zeolites are capable of stabilizing rhodium carbonyl species with increasing oxidation state. With the precursors starting with $1^+$, $2^+$, or $3^+$ oxidation states, this idea is important. The peaks that do appear are again small, but never-the-less distinguishable and show up in five of the six catalysts with Si/Al ratios of 23 and 50, while none are present in the Si/Al 280 samples. The peaks corresponding to Rh(II)-CO are 2139-2144 and 2174-2177 $cm^{-1}$, with a frequency for Rh(III)-CO occurring at 2168 $cm^{-1}$.[28, 30] The Rh(II)-CO species are seen in Si/Al 23:Rh(I), Si/Al 23:Rh(II), Si/Al 50:Rh(II), Si/Al 23:Rh(III), and Si/Al 50:Rh(III). Only one catalyst, Si/Al 23:Rh(I), shows any stability for the Rh(III)-CO state, although it is noted that the frequency is close to Rh(II)-CO so it could just be a slight shift that is

seen. Comparing the peak intensities yields a similar result as above, with catalysts of Si/Al 23 showing better stability than the Si/Al 50 catalysts and Si/Al 280 samples having no such bonds present. The Si/Al 23:Rh(III) catalyst shows a unique structure in that the intensity of the peaks attributed to Rh(II)-CO are almost as great as those for Rh(I)-CO. During synthesis of the catalyst the rhodium is able to bond to the zeolite and retain its properties without reducing to $Rh^{1+}$.

## 2.5 Conclusions

Anchoring rhodium into the pores of zeolite ZSM-5 is studied via CO adsorption to determine the resulting effect from changing the Si/Al ratio. Dicarbonyl ligands attached to Rh(I) are the main species in all catalysts, with the distinguishing characteristics being their ability to coordinate unique tricarbonyl or tetracarbonyl ligands to Rh(I) or stabilize Rh(II)-CO or Rh(III)-CO. When comparing the data across the three rhodium precursors, having a higher $Al^{3+}$ content (Si/Al 23) leads to greater stability of the less prevalent species when compared to Si/Al 50 catalysts. Catalysts synthesized using ZSM-5 with Si/Al 280 do not form bonds other than the $Rh^{1+}(CO)_2$. Looking at the presence of tricarbonyl and tetracarbonyl species versus the presence of higher oxidation rhodium complexes, the precursors using Rh(II) and Rh(III) always show the ability to stabilize complexes of Rh(II)-CO, whereas the catalysts using the Rh(I) precursor do not always show this trait but do have the more coordinated species.

## Chapter 3: X-Ray Absorption Spectroscopy

### 3.1 Abstract

When looking at XAS data, changing the Si/Al ratio and rhodium precursors show marked differences. For catalysts synthesized using the Rh(I) precursor, a cluster of two atoms is present, while catalysts using the Rh(II) precursor stabilize in a cluster of four or six atoms. Also, differences in Rh-Rh bond length show the effects on contraction or expansion of the clusters due to Si/Al ratio. XANES data shows changes in the oxidative environment among the Si/Al ratios for the Rh(I) series of catalysts, while a more reduced environment is visible for all Rh(II) series catalysts.

### 3.2 Introduction

Using X-ray absorption spectroscopy (XAS), additional information about the active centers of catalysts can be discovered. XANES plots give information about the oxidative environment around the rhodium center, and monitor the structure change as treatments are used. More specific information about the structure is found using EXAFS, as coordination number and nearby atoms are shown. From this the exact structure of the active species can be determined. Anchoring metals inside zeolite pores can lead to mononuclear sites or small clusters of 6 or fewer atoms which are able to be stabilized. Changes in XAS data due to Si/Al ratio and precursor structure

will be observed, which is particularly important given that multiple rhodium precursors are used, with the structures having very different orientations to begin with.

### 3.3 Experimental

X-ray absorption spectroscopy experiments were performed at beamlines X11A and X18B of the National Synchrotron Light Source (NSLS) at Brookhaven National Lab, New York. The ring current was 2.8 GeV with an intensity of 300-165 mA. A double-crystal Si(111) monochromator was used, with detuning of 20% to suppress higher harmonics in the X-ray beam. All samples were scanned at the Rh K edge (23,220 eV) in transmission mode, with the sample in a custom-made XAS cell; samples were scanned 3-5 times and then averaged for data analysis.

Analysis of the EXAFS data is carried out using a difference file technique [31, 32] with the software XDAP;[33] reference files are obtained using the software FEFF 7.0 or 8.0.[34, 35] No attempt is made to account for the small atomic X-ray absorption fine structure,[36, 37] data obtained at low values of r, other than by application of standard background removal techniques.[38] Iterative fitting was carried out until excellent agreement was attained between the calculated $k^0$-, $k^1$-, and $k^2$- weighted data and the model. The quality of the fitting was confirmed by the values of fit diagnostic parameters, $\varepsilon^2\nu$ (goodness of fit), and the variances between

the data and the model prediction for the EXAFS function $\chi$ and the Fourier transform of $\chi$.

### 3.4 Results and Discussion

XANES and EXAFS data were collected under two conditions: the fresh catalyst samples, and then after thermal treatment in He. Comparisons are made between the two conditions to look at stability of the active site and to find the working structure of the catalyst. Figures 3.1-3.3 show XANES data for the Rh(I) series of catalysts with ZSM-5 Si/Al 23, 50, and 280.

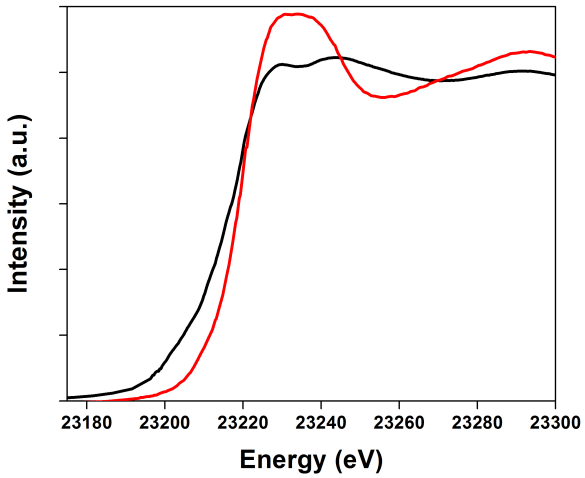


**Figure 3.1. XANES plot for the Si/Al 23:Rh(I) catalyst showing the fresh catalyst (black) and after thermal treatment in He (red).**

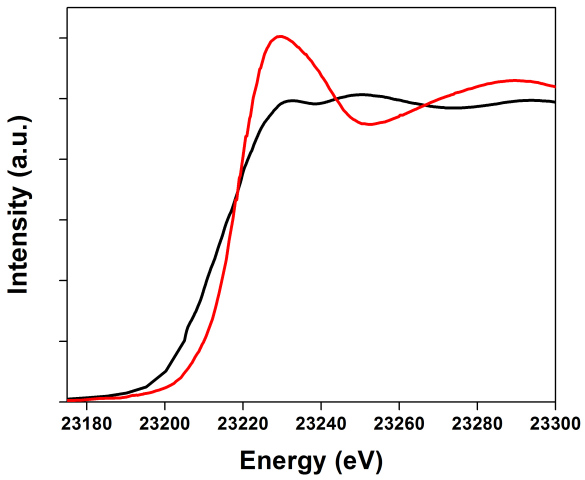


**Figure 3.2. XANES plot for the Si/Al 50:Rh(I) catalyst showing the fresh catalyst (black) and after thermal treatment in He (red).**

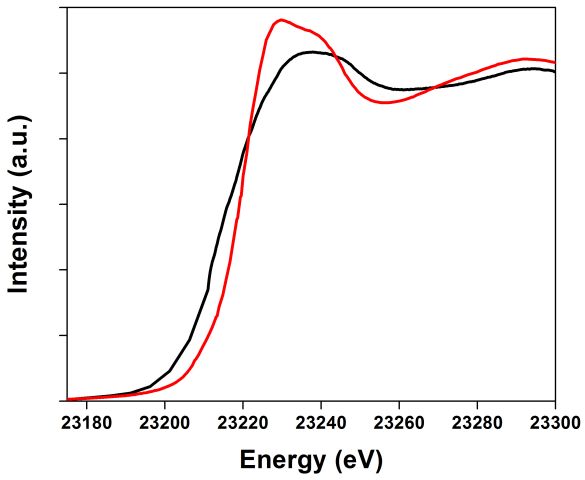


**Figure 3.3. XANES plot for the Si/Al 280:Rh(I) catalyst showing the fresh catalyst (black) and after thermal treatment in He (red).**

For both the Si/Al 23-Rh(I) and Si/Al 50-Rh(I) fresh catalysts and the treated Si/Al 280-Rh(I) sample, there are two peaks, one at 23,230 and the other appearing at

23,245 eV. This shape is found in literature,[39, 40] and is attributed to an oxidized catalyst. For the Si/Al 23-Rh(I) and Si/Al 50-Rh(I) treated catalysts, and the fresh Si/Al 280-Rh(I), the XANES plot shows one peak. A single peak such as this is also reported in literature,[39] and it too is attributed to an oxidized rhodium species. Although both the fresh and treated plots for all samples are attributable to oxidized species, the extent to which each is oxidized varies. The plots showing the more oxidized environment are those with one prominent single peak; this main peak height will decrease followed by the appearance of a second peak as a sample is slowly reduced.[39] Therefore, the thermal treatment of each of the samples for the Rh(I) series changes the anchoring of the rhodium to the zeolite such that the rhodium is now in a more oxidative environment. Also, comparing just the treated catalysts, each of the Si/Al ratios lead to different XANES plots. Although there is just one peak, the shape of each peak shows variation; therefore, Si/Al ratio does affect the way in which the rhodium bonds to the zeolite.

Similarly, XANES data for the Rh(II) precursor series are shown in Figures 3.4-3.6. All data for the fresh samples are similar, with one broad peak present, again attributable to oxidized rhodium. For the Si/Al 280-Rh(II) catalyst, treatment in He does not have a significant effect on the Rh. However, after thermal treatment in He, substantial differences are seen for Si/Al 23-Rh(II) and Si/Al 50-Rh(II). In both cases, the data shows two prominent peaks; they are however distinguishable from the two peaks in the fresh catalysts of the Rh(I) series. These samples are more

similar to XANES data of metallic Rh; Figure 3.7 shows the two treated catalysts alongside Rh foil.

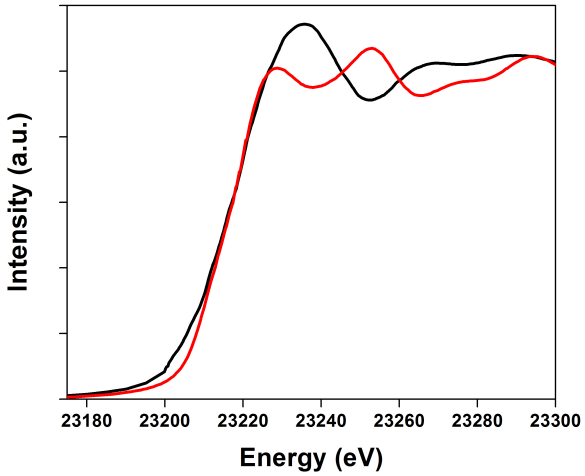


**Figure 3.4. XANES plot for the Si/Al 23:Rh(II) catalyst showing the fresh catalyst (black) and after thermal treatment in He (red).**

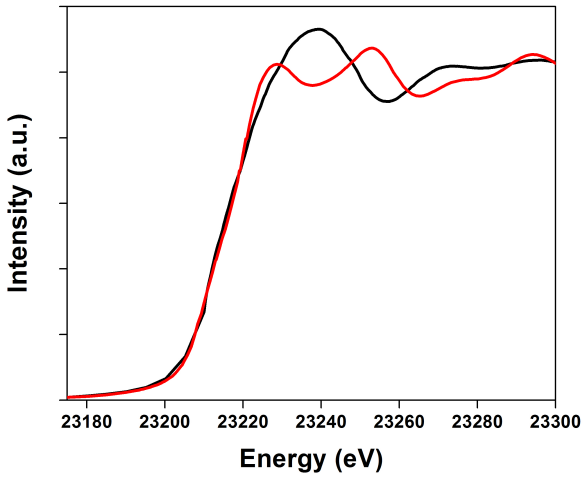


**Figure 3.5. XANES plot for the Si/Al 50:Rh(II) catalyst showing the fresh catalyst (black) and after thermal treatment in He (red).**

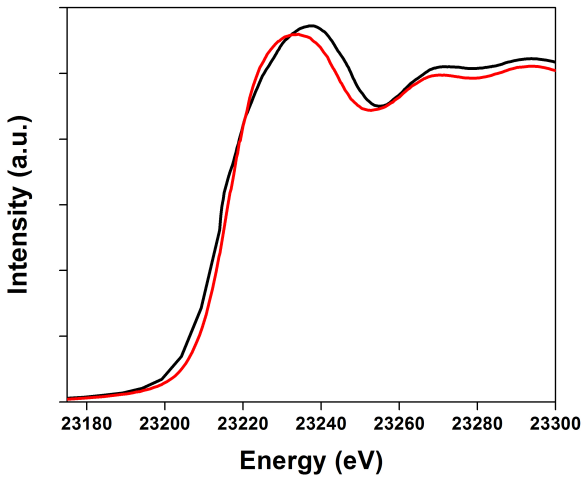


**Figure 3.6. XANES plot for the Si/Al 280:Rh(II) catalyst showing the fresh catalyst (black) and after thermal treatment in He (red).**

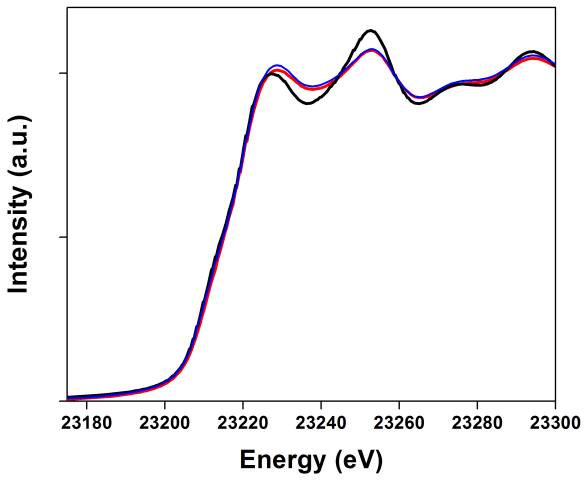


**Figure 3.7. Comparison of Si/Al 23:Rh(II) (red) and Si/Al 50:Rh(II) (blue) versus metallic rhodium (black).**

Although similar, the heights of the two peaks with respect to the metal rhodium data show important differences. Both Si/Al 23-Rh(II) and Si/Al 50-Rh(II) treated

samples have shallower valleys between the two peaks, and the second peaks are also of lower intensity. This filling in of the valley and less intense second peak for the XANES plots is attributable to an increase in oxidation state compared to metallic rhodium.[39] There is a possible mixture of metallic rhodium and cationic rhodium species after thermal treatment for the Si/Al 23-Rh(II) and Si/Al 50-Rh(II) samples.

EXAFS data of the fresh catalysts confirms the presence of the rhodium in its original state. For the catalysts using the Rh(I) precursor, there is a single Rh atom with two carbonyl ligands still attached. The Rh(II) precursor samples show the rhodium dimer structure still intact. Thus, initially, rhodium has gone into the zeolite pore and anchored around the Al atom.

EXAFS data is also available after the thermal treatment in He. This data will show how rhodium anchors and stabilizes in the ZSM-5 pore before use in the reaction. Figures 3.8 and 3.9 show the chi and Fourier Transform plots for the Si/Al 23:Rh(II) sample; the red line in each case shows how close of a fit the model gives. The results of the model fitting are enumerated in Table 3.1. EXAFS chi and FT plots for the rest of the catalysts are included in the Appendix.

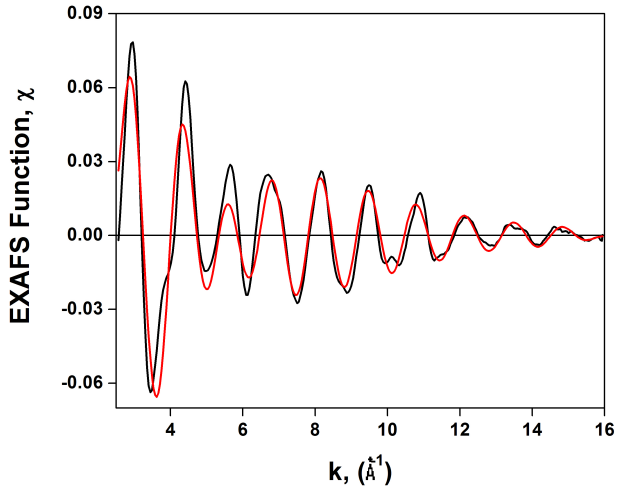


**Figure 3.8. The chi plot of catalyst Si/Al 23:Rh(II), showing the fit of the model (red) versus the experimental data (black).**

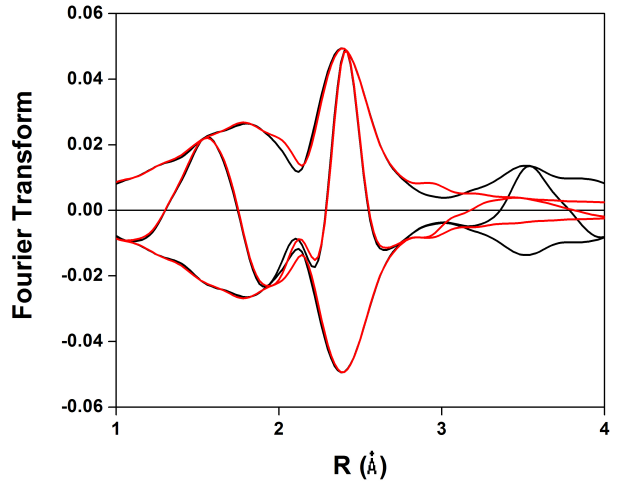


**Figure 3.9. The Fourier Transform plot of catalyst Si/Al 23:Rh(II), showing the fit of the model (red) versus the experimental data (black).**

**Table 3.1. Results from the XDAP program for Rh(I) and Rh(II) catalysts after thermal treatment, showing coordination number (N) and bonding distance (R) which fit the experimental EXAFS data.**

| Si/Al 23 : Rh(I) | | |
|---|---|---|
| Contribution | N | R (Å) |
| Rh - RH | 1 | 2.72 |
| Rh - O | 4 | 1.99 |
| Rh - Al | 0.5 | 2.8 |

| Si/Al 50 : Rh(I) | | |
|---|---|---|
| Contribution | N | R (Å) |
| Rh - RH | 1 | 2.66 |
| Rh - O | 4 | 2.05 |
| Rh - Al | 1 | 2.89 |

| Si/Al 280 : Rh(I) | | |
|---|---|---|
| Contribution | N | R (Å) |
| Rh - RH | 1 | 2.72 |
| Rh - O | 2.5 | 2.09 |
| Rh - Al | 1 | 2.85 |

| Si/Al 23 : Rh(II) | | |
|---|---|---|
| Contribution | N | R (Å) |
| Rh - RH | 3 | 2.67 |
| Rh - O | 1 | 2.11 |
| Rh - Al | 1 | 2.84 |

| Si/Al 50 : Rh(II) | | |
|---|---|---|
| Contribution | N | R (Å) |
| Rh - RH | 3 | 2.66 |
| Rh - O | 1 | 2.11 |
| Rh - Al | 1 | 2.84 |

| Si/Al 280 : Rh(II) | | |
|---|---|---|
| Contribution | N | R (Å) |
| Rh - RH | 1 | 2.65 |
| Rh - O | 4 | 2.04 |
| Rh - Al | 1 | 2.79 |

Comparing the Rh(I) series catalysts, thermal treatment substantially alters the overall structure of the rhodium site with differences also present due to changes in Si/Al ratio. Each of the three catalysts now has 1 Rh-Rh bond; initially, only monatomic rhodium sites were observed but the He treatment results in a two atom cluster. Looking at the Rh-Rh bonding distance, both Si/Al 23:Rh(I) and Si/Al 280:Rh(I) catalysts have 2.72 Å bonds while the Si/Al 50:Rh(I) sites have a length of 2.66 Å. These are all in line with appropriate Rh bond lengths. However, a difference of 0.06 Å shows a much shorter and more compact dimer structure for Si/Al 50:Rh(I), the change in Si/Al ratio clearly has an effect. Each of the catalysts is anchored around an Al atom, as is expected, although Si/Al 23:Rh(I) has a coordination of only 0.5. With two Rh atoms, this could be explained in the orientation of the dimer where only one of the Rh atoms is positioned close to the Al while the other is not. A significant number of oxygen atoms are also in close proximity; Si/Al 23:Rh(I) and Si/Al

50:Rh(I) have a coordination number of 4 with Si/Al 280:Rh(I) at 2.5. These oxygens can be attributed to the framework oxygens and provide an important reference point when determining the orientation of the dimer structure within the ZSM-5 pores. Because of the symmetrical structure of ZSM-5, four main acid sites are presented as the most stable and viable options, with their structures shown in Figure 3.10. Ring a of the figure is the main pore channel opening which runs through ZSM-5, with rings b, c, and d along the wall of the main channel. For catalysts Si/Al 23:Rh(I) and Si/Al 50:Rh(I) four oxygens surround each Rh atom in the dimer structure, so positions b-d on the channel wall are viable anchoring sites. Although four oxygens surround each Rh atom, the number of oxygens which actually bond to rhodium are not ascertainable from EXAFS data. For the Rh dimer two main options exist: both Rh atoms are bonded to framework oxygens, or one of the Rh atoms is bonded while the other is free. The Si/Al 280:Rh(I) sample has a coordination number of 2.5, indicating that the Rh dimer is in a different environment than the other two Si/Al ratios. With fewer oxygen atoms, it would be possible to anchor to the main pore opening (a).

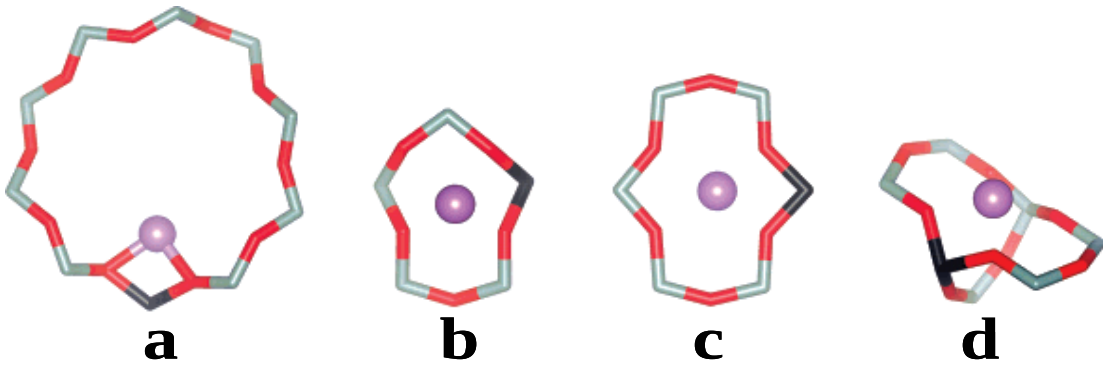


**Figure 3.10. Possible locations to anchor the rhodium clusters within ZSM-5. The framework Al, Si, and O atoms are represented via black, gray, and red colors. The purple ball would be the approximate location of the cluster. Site a corresponds to the main 10-member channel and sites b-d are six-member rings along the main channel wall.[41]**

Comparing the Rh(II) precursor catalysts, the results for Si/Al 23 and 50 are similar, with the Si/Al 280 catalyst having distinct results. With a coordination number of 3 for the Rh-Rh shell, this shows that a small cluster of four rhodium atoms has now formed. Or, two dimers from the original species have joined together. Of note is the idea that it could be attributed to either a four or six atom Rh cluster. There are articles which report a coordination of 3, but explain this as an overall six atom species.[42-44] The full cluster of Rh atoms would essentially block the view, so that any one individual Rh atom would only see its three nearest neighbors. In these articles, they are also starting with a six Rh atom species, which is how they are able to explain the EXAFS data. For this research, it is not possible to fully determine whether or not the final complex is four or six atoms, but it is one of the two; both structures are seen as stable and viable options. The Rh bonding distance for Si/Al 23:Rh(II), Si/Al 50:Rh(II), and Si/Al 280:Rh(II) start at 2.67 Å and decrease by 0.01

Å with increasing Si/Al ratio. There is not as much of a length difference as seen in the Rh(I) catalysts, but slight distortions are noticeable. Additionally, one oxygen atom and one aluminum atom are near rhodium atoms for Si/Al 23:Rh(II) and Si/Al 50:Rh(II) while Si/Al 280:Rh(II) has four oxygens and one aluminum atom close to the rhodium. With these Rh(II) series catalysts having an overall larger and more complex structure it is harder to pinpoint the orientation and location of the molecule to a specific site in Figure 3.10. Though looking at the four atom complex with a trigonal pyramidal structure, there is the potential that it could be arranged within any of the locations.

### 3.5 Conclusions

Initially, all catalysts synthesized with the Rh(I) precursor do not show any Rh-Rh bonds, and the basic structure of the precursor is intact, although bonded in close proximity to an Al atom. After thermal treatment in He, each of the catalysts formed a different complex with changes in the oxidative environment and structure. Each of the three Si/Al ratios of the Rh(I) series has an oxidative environment as seen in XANES data; the peak shape in each plot is different showing that changing the Si/Al ratio has an affect. Furthermore, EXAFS data presents a structure where two Rh atoms are now bonded, but with clear differences in bond lengths. While Si/Al 23:Rh(I) and Si/Al 280:Rh(I) have the same Rh-Rh bond lengths, a contraction of 0.06 Å is visible for the Si/Al 50:Rh(I) sample which is a significant change.

Although it is not possible to discern exactly which acid site each anchors to, due to the presence of four oxygen atoms in EXAFS data for Si/Al 23:Rh(I) and Si/Al 50:Rh(I), these two catalysts would only see such an environment if anchored inside the channel wall. For Si/Al 280:Rh(I) it is possible to bond to the channel opening as there are only 2.5 oxygens in close proximity.

The catalysts utilizing the Rh(II) precursor have the rhodium dimer still intact in the fresh sample with cationic rhodium present. Comparatively, both Si/Al 23:Rh(II) and Si/Al 50:Rh(II) catalysts stabilize in a cluster of four or six atoms after thermal treatment ,while Si/Al 280:Rh(II) stays intact as the initial dimer structure. Through XANES data, each catalyst has a more reduced environment than initially, so both cationic and metallic rhodium species are present. Due to differences in the rhodium precursor and size of the cluster for Rh(II) catalysts, the rhodium may not be as stable in an oxidized form, and would reduce to its metallic form. Changing the Si/Al ratio for this precursor leads to small distortions in the structure, as the Rh-Rh bond length is only 0.01 Å shorter.

A note must be included when trying to distinguish whether Rh is present in its oxidized or reduced form and to what extent. X-ray absorption spectroscopy is an averaging technique, which looks at each individual Rh atom available in the catalyst. If both metallic and cationic rhodium is present, this could not be distinguished through the XAS data. Likewise, with clusters of Rh present, each Rh will not have

the exact same neighbor atoms. For instance, a bond to the zeolite pore framework exists, but in a cluster not every Rh atom would be attached to it, rather only one or two would be bonded. This has an affect both on coordination number and on bond distance. If there were minor structural differences between active sites or slight oxidation changes, XAS would not be able to detect this. The main active site structure, however, is still clearly discernable.

# Chapter 4: Hydrogen Production from Methanol

## 4.1 Abstract

The partial oxidation of methanol is investigated, comparing hydrogen production with Si/Al ratio. Due to issues with the reaction setup, however, there is limited data. For Si/Al 23 and Si/Al 50 catalysts, there are results which show minimal differences in hydrogen production and therefore little impact on the reaction. But data is also present where using ZSM-5 with either Si/Al 23 or Si/Al 50 will produce much more hydrogen, and thus the full evaluation of these results is not able to be determined at this point. Catalysts which use ZSM-5 with Si/Al 280 as the support have negligible hydrogen production, however.

## 4.2 Introduction

Now that the catalysts have been characterized using IR and XAS spectroscopic techniques, it is necessary to test each of them in a reaction. The spectroscopies show us the structural and environmental differences between each catalyst, and the reaction testing will illustrate how these differences affect the reaction; or which combination of zeolite ZSM-5 Si/Al ratio and precursor is more favorable. The ability to produce alternative energy sources is of paramount importance, and using methanol to produce hydrogen for use in PEM fuel cells is a leading candidate. This

study will focus on the partial oxidation of methanol using $O_2$ as the oxidant and comparisons will be made based on the amount of hydrogen produced.

## 4.3 Experimental

To bring methanol in contact with the catalyst, He (Airgas) flows through a saturator filled with methanol with the outlet gas having a concentration of 5% methanol. An appropriate flowrate of $O_2$ (Airgas) is used such that oxygen is in excess, with a molar ratio for $O_2$:$CH_3OH$ of 7:1. The catalyst is pressed into .015 g wafers which are placed into the reactor cell used in conjunction with the Bruker Optics FTIR. The outlet gasses are sent to a Pfeiffer Vacuum OmniStar mass spectrometer to be analyzed as the reaction proceeds. For each catalyst run, the reaction is started at room temperature and then increased and held at temperatures of 125 °C, 150 °C, 175 °C, 200 °C, and 225 °C.

## 4.4 Results and Discussion

For each run, IR data was taken to watch the appearance of peaks both before the reaction takes place and then also at high temperatures. When at room temperature, the methanol starts to adsorb to the catalyst, as seen in Figure 4.1.

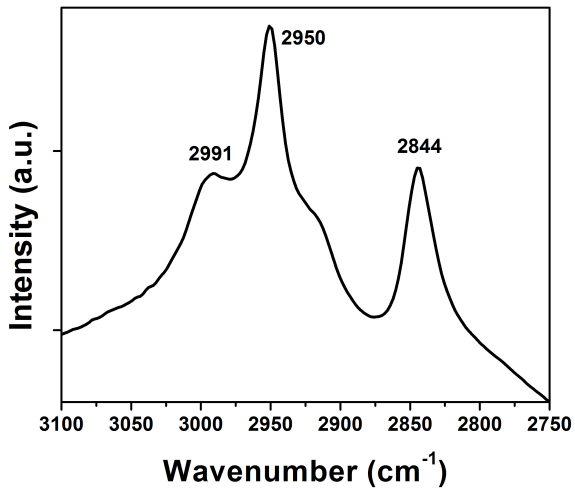


**Figure 4.1. Methanol adsorption on the catalyst, showing both physical and chemisorption.**

There are three peaks, with 2844 and 2950 $cm^{-1}$ attributable to the physical adsorption of the $CH_3OH$ species. Chemisorption is also seen through the presence of a methoxy species, $CH_3O^-$, at 2991 $cm^{-1}$.

The reaction proceeds minimally until reaction temperatures of 175-200 °C are reached. This is evidenced by the appearance of CO bands as methanol decomposes on catalysts synthesized using the Rh(I) precursor, as shown in Figure 4.2 at 175 °C; before this temperature no such peaks are present.

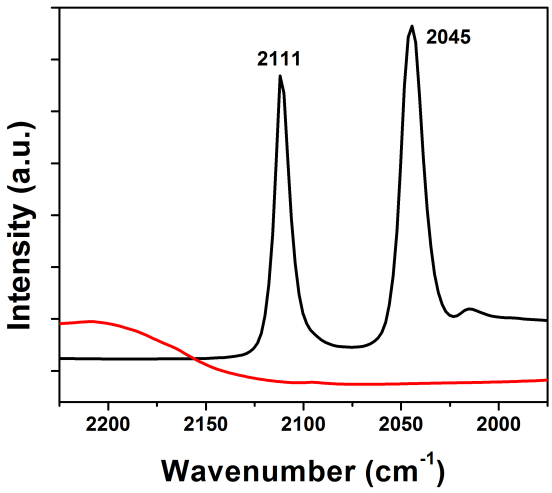


**Figure 4.2. IR data taken during the reaction of methanol when using catalysts synthesized using the Rh(I) precursor, showing the presence of CO peaks. The red line is at room temperature with the black line at a reaction temperature of 175 °C.**

In addition to showing when the reaction begins, much more can be gleamed from this data when the CO peaks are compared to the IR data from chapter 2. Those CO adsorption studies showed the presence of two main peaks attributable to $Rh^{1+}(CO)_2$ at 2115 and 2048 $cm^{-1}$. The CO peaks which appear during methanol decomposition here are very close, with frequencies of 2111 and 2045 $cm^{-1}$. A redshift occurs for both peaks to lower energies, but methanol and $O_2$ are also present and interacting with Rh in the reaction which would change the electronic density accounting for this change. This data would then go towards showing the stability of the active rhodium center, even during participation in the reaction, as the same or at least very similar rhodium species are present; oxidized rhodium is available and is not reduced. This is promising, since active centers before and during a reaction are not always necessarily the same.

These CO peaks are only seen, however, on the catalysts which use the Rh(I) precursor, and not on the catalysts with the Rh(II) precursor. This could mean one of two ideas. One is that a CO is not on the Rh for as long or methanol interacts in a different manner with these precursors, so that CO would not be detected with the IR. With the active centers showing very different cluster sizes and the mechanism of the reaction not investigated, this is possible. The other is that the presumed active center is not stable and reduces to a different structure during the reaction. In order to answer this question, further testing would be warranted.

Knowing that the catalysts are indeed reacting with and decomposing the products and show signs of having a similar structure as before hand, each catalyst is compared looking at hydrogen production. The data for each catalyst tested for the production of hydrogen via partial oxidation of methanol is shown in Figures 4.3 and 4.4; Figure 4.3 shows the data for the catalysts synthesized using the Rh(I) precursor while Figure 4.4 has all Rh(II) catalysts. For some catalysts, two experimental runs are shown and are denoted as “a” and “b” in the plots; these show differences seen for the same catalyst, this is detailed in the following paragraphs.

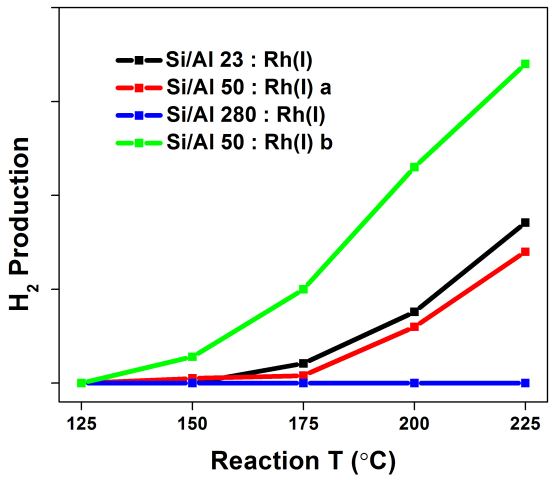


**Figure 4.3. Hydrogen production for catalysts using Rh(I) precursor.**

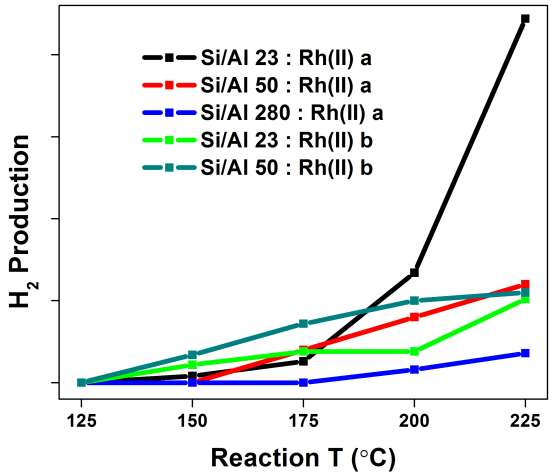


**Figure 4.4. Hydrogen production for catalysts using Rh(II) precursor.**

In both sets of reaction data, the catalysts using ZSM-5 of Si/Al 280 show minimal hydrogen production. The Si/Al 280:Rh(I) catalyst does not produce hydrogen at any temperature tested. Likewise, Si/Al 280:Rh(II) has a very modest gain but is small

compared to the initial value. Having too large of a Si/Al ratio has a detrimental effect on the reaction.

Comparing Si/Al ratios of 23 and 50 for both sets of catalysts shows mixed results, with two explanations given. Looking at Figure 4.3, runs Si/Al 23:Rh(I) and Si/Al 50:Rh(I)a show almost identical results. This also holds true in Figure 4.4, when comparing runs Si/Al 23:Rh(II)b, Si/Al 50:Rh(II)a, and Si/Al 50:Rh(II)b. From this it could be postulated that Si/Al ratio does not have an effect on the partial oxidation of methanol. As long as the Si/Al ratio is such that enough Bronsted acid sites are available, the differences in structure when rhodium is anchored have a limited effect and the reaction will produce hydrogen at a set rate.

However, a differing trend among hydrogen production data is also seen in both figures. In Figure 4.3, Si/Al 50:Rh(I)b data would suggest that increasing the Si/Al ratio leads to better production. While in Figure 4.4, Si/Al 23:Rh(II)a has a substantial increase, so it could be proposed that a lower Si/Al ratio is better for $H_2$ production. Since two different rhodium precursors are being used, it is not necessary that they both show the same effects on the reaction. Looking at the EXAFS results, the catalysts using the Rh(I) precursor have an active site of two Rh atoms, while the samples using Rh(II) precursor have 4-6 atoms at the reaction site. Therefore, it is reasonable that the reaction would proceed differently with respect to Si/Al ratio. Unfortunately, the discrepancies in the data are not able to be fully sorted out; the

reaction setup stopped working properly, and the source of the problem was not found so further reactions were not able to be tested.

### 4.5 Conclusions

The partial oxidation of methanol using the proposed rhodium catalysts is showing mixed results to this point with respect to Si/Al ratio. A portion of the data for catalysts using Si/Al 23 and 50 shows comparable results for hydrogen production. Thus, it would be concluded that there is no effect on $H_2$ production by changing the number of aluminum sites. However, data points are also present which show much higher production rates. The catalysts Si/Al 50:Rh(I)b and Si/Al 23:Rh(II)a both show a propensity for much greater hydrogen production. Whether these runs are simply outliers are not able to be determined at this point however. What is known is that all catalysts with Si/Al 280 show negligible hydrogen production. The number of Al sites is too small, such that anchoring rhodium is not conducive to producing sites where reactions occur or the number of sites is too few.

This idea is further expounded upon with relation to the active site for the reaction; whether or not methanol reacts on the rhodium sites or simply on the Bronsted acid sites present within the ZSM-5. As seen in the reaction data, the Rh(I) catalysts show the Si/Al 50 sample with the best potential for maximum $H_2$ production, while for Rh(II) catalysts the potential was greater for Si/Al 23. Even with no background data

available for the bare zeolite to determine how much, if any, of the $H_2$ production is due to the bronsted acid sites alone, it can be concluded that the anchoring of rhodium does play a role. If in fact the reaction only took place at the acid sites, this would lead to both Si/Al 23 catalysts always having the greatest $H_2$ production. Since the Rh(II) catalyst with Si/Al 50 shows better $H_2$ production than its Si/Al 23 counterpart, rhodium does have a promotion effect and plays a part in the methanol oxidation reaction.

IR data taken during the experiments have very intriguing results which show that rhodium is present in its oxidized $Rh^{1+}$ form during reaction when using the Rh(I) precursor, the same as before the reaction started. This shows that the anchoring of rhodium is a stable process for these catalysts. These CO peaks are not present when reacting the catalysts synthesized using the Rh(II) precursor.

## Chapter 5: Project Summary

### 5.1 Conclusions

To characterize rhodium anchored on ZSM-5, IR and XAS spectroscopic techniques were utilized. These spectroscopies show changes due to different Si/Al ratios and rhodium precursors. The partial oxidation of methanol is then investigated to determine their effect on the reaction.

IR CO adsorption studies establish differences in both ligand and oxidation environments. For all catalysts, a main species of $Rh^{1+}(CO)_2$ is present, however, Rh(II)-CO and Rh(III)-CO species are visible, along with tricarbonyl and tetracarbonyl ligands depending on the Si/Al ratio. The Si/Al 23 catalysts stabilize the high oxidation and multiple ligand species to a greater degree than Si/Al 50 and Si/Al 280 samples. Catalysts using ZSM-5 with Si/Al 50 still show an ability to stabilize a small amount of these lesser species, with Si/Al 280 only showing $Rh^{1+}(CO)_2$. Increasing the rhodium precursor oxidation state also shows a greater ability to stabilize more oxidative rhodium.

The structure of the rhodium site when immobilized inside the zeolite pore is established with XAS for the Rh(I) precursor catalysts. While initially monatomic rhodium is present for Rh(I) precursor catalysts, this is not stable and after thermal

treatment in He a cluster of two Rh atoms is distinguishable. Comparing the bond lengths from EXAFS, Si/Al 50:Rh(I) has a much more compact structure clearly showing an affect from changing the Si/Al ratio. Although the reaction data has inconclusive results, the Si/Al 50:Rh(I) catalyst is one which has an increase in hydrogen production; therefore, a shorter Rh-Rh bond could benefit the reaction. Also, CO peaks during the partial oxidation reaction have similar frequencies to those ascertained during CO adsorption studies, showing this as a stable, active site for reaction. A consistent active site of two cationic rhodium atoms anchored in the ZSM-5 pore demonstrates the idea of having a uniform, single-site catalyst.

XAS experiments also establish the structure of Rh(II) precursor catalysts. When using the Rh(II) precursor, its dimer structure is intact for the fresh catalysts, with a four or six atom cluster visible after thermal treatment. The bond lengths among the Si/Al ratios for the Rh(II) series catalysts do not have as substantial of a change, but do show 0.01 Å decreases. While IR studies establish the presence of oxidized rhodium for all Rh(II) precursor catalysts, XANES experiments reveal a more reduced rhodium. Both metallic and cationic rhodium may stabilize in the catalyst. If this is true, the idea of having a uniform, single-site catalyst may not hold for this series of catalysts, and rather a mixture of rhodium sites may exist.

Comparing both XAS and IR data simultaneously when reviewing the differences seen in the catalysts is critical, especially when trying to conclude how this affects the

reaction. If looking exclusively at XAS data, large and extravagant changes in the structure are not seen, and thus it could be reasoned that similar species are present on each catalyst regardless of Si/Al ratio. Coupling this with IR data, which shows distinct differences in the type of rhodium species present, the full story starts to emerge. If multiple rhodium species are present with difference oxidation states or coordination, this is harder to see in XAS due to its averaging technique. The dominant species present would in essence block out any minor rhodium species, even though they are available. Keeping this in mind is important when looking at the methanol oxidation results, which do appear to show differences with Si/Al ratio. Although perhaps a similar rhodium structure exists in all catalysts, the presence of minor rhodium species could play an important rule in the reaction and substantially change the results.

A final thought is also warranted when looking at the structure of the Si/Al 280:Rh(II) catalyst in relation to its similarity to Rh(I) catalysts. Sample Si/Al 280:Rh(II) in the end is still in its dimer structure, and is the only catalyst which does not show a growth in cluster size after thermal treatment. The Rh(II) precursor is very different than the Rh(I) precursor, in both the number of rhodium atoms present and in its ligand structure. It would be anticipated that this would have substantial effect on its final form. Looking at the Rh-Rh bond lengths allows for further discussion; the Rh-Rh lengths are 2.65 Å for Si/Al 280:Rh(II) versus lengths of 2.72 Å for Si/Al 23:Rh(I), 2.66 Å for Si/Al 50:Rh(I), and 2.72 Å for Si/Al Rh(I). The Rh-Rh length

for Si/Al 280:Rh(II) and Si/Al 50:Rh(I) are similar, while the other catalysts have longer bonds. The difference for the Si/Al 50:Rh(I) sample is attributed to an effect from the Si/Al ratio, but this cannot necessarily be the argument for the Si/Al 280:Rh(II) sample, especially as it relates to Si/Al 280:Rh(I). The difference is then attributed to the rhodium precursor. The Rh(II) precursor dimer initially has a Rh-Rh bond length of 2.39 Å. Although it does not retain its compacted rhodium dimer size, it still has an overall effect, as it does lead to structures with shorter bonds, and the shorter bonds are present throughout all Rh(II) catalysts. This shows that in addition to the Si/Al ratio, the initial structure of the rhodium plays a role.

## 5.2 Recommendations

The first order of business would be to run additional reaction experiments, to elucidate the actual trend when comparing Si/Al ratio. Knowing whether or not the same Si/Al ratio leads to better conversion when comparing the two rhodium precursors is intriguing, if in fact a Si/Al ratio of 23 works better for the Rh(II) precursor series while for the Rh(I) precursor series the Si/Al 50 ratio is better, this would open the doors for further research to explain this phenomenon. Also, reaction data for the bare zeolite is needed to make comparisons against the Rh on ZSM-5 catalysts. This would help in showing the benefit from anchoring the rhodium inside the zeolite pores, versus the reaction taking place only at Bronsted acid sites.

Gathering XAS data under reaction conditions would also be helpful. As is seen in Figure 4.2, IR data shows the presence of $Rh^{1+}(CO)_2$ species, having XANES and EXAFS to corroborate the structure would further prove the stability of the rhodium site. Along with this, in order to specifically establish the way in which the clusters bond inside the zeolite, it would be necessary to perform theoretical calculations. Density functional theory (DFT) is commonly seen in journal articles as a tool to identify the best possible candidates for the structure of the active site. For this research, answering the question of how the rhodium clusters bond to the framework oxygens would provide valuable insight into the working catalyst.

## References


1. Harrison, K. *Zeolite ZSM-5*. 1997 [cited 2008; Available from: http://www.3dchem.com/molecules.asp?ID=86.
2. Haw, J.F., *Zeolite acid strength and reaction mechanisms in catalysist.* Physical Chemistry Chemical Physics, 2002. **4**(22): p. 5431-5441.
3. Maschmeyer, T., et al., *Heterogeneous Catalysts Obtained by Grafting Metallocene Complexes onto Mesoporous Silica.* Nature, 1995. **378**(6553): p. 159-162.
4. Shannon, I.J., et al., *Metallocene-derived, isolated Mo-VI active centres on mesoporous silica for the catalytic dehydrogenation of methanol.* Journal of the Chemical Society-Faraday Transactions, 1998. **94**(10): p. 1495-1499.
5. Thomas, J.M. and R. Raja, *Significance of mesoporous crystals for catalytic application.* Mesoporous Crystals and Related Nano-Structured Materials, 2004. **148**: p. 163-211.
6. Coperet, C., et al., *Homogeneous and heterogeneous catalysis: Bridging the gap through surface organometallic chemistry.* Angewandte Chemie-International Edition, 2003. **42**(2): p. 156-181.
7. Ahn, H. and T.J. Marks, *High-resolution solid-state C-13 NMR studies of chemisorbed organometallics. Chemisorptive formation of cation-like and alkylidene organotantalum complexes on high surface area inorganic oxides.* Journal of the American Chemical Society, 2002. **124**(24): p. 7103-7110.
8. Ahn, H., C.P. Nicholas, and T.J. Marks, *Surface organozirconium electrophiles activated by chemisorption on "super acidic" sulfated zirconia as hydrogenation and polymerization catalysts. A synthetic, structural, and mechanistic catalytic study.* Organometallics, 2002. **21**(9): p. 1788-1806.
9. Nicholas, C.P., H.S. Ahn, and T.J. Marks, *Synthesis, spectroscopy, and catalytic properties of cationic organozirconium adsorbates on "super acidic" sulfated alumina. "Single-site" heterogeneous catalysts with virtually 100% active sites.* Journal of the American Chemical Society, 2003. **125**(14): p. 4325-4331.
10. Thomas, J.M., et al., *High-performance nanocatalysts for single-step hydrogenations.* Accounts of Chemical Research, 2003. **36**(1): p. 20-30.
11. Knopsgerrits, P.P., et al., *Zeolite-Encapsulated Mn(Ii) Complexes as Catalysts for Selective Alkene Oxidation.* Nature, 1994. **369**(6481): p. 543-546.
12. Zsigmond, A., et al., *Ruthenium-catalyzed aerobic oxidation of alcohols on zeolite-encapsulated cobalt salophen catalyst.* Topics in Catalysis, 2002. **19**(1): p. 119-124.
13. Goellner, J.F., et al., *Structure and bonding of a site-isolated transition metal complex: Rhodium dicarbonyl in highly dealuminated zeolite Y.* Journal of the American Chemical Society, 2000. **122**(33): p. 8056-8066.

14. Enderle, B. and B.C. Gates, *Alkene hydrogenation catalyzed by rhenium carbonyls bonded to highly dealuminated Y zeolite: spectroscopic characterization of the working catalyst.* Journal of Molecular Catalysis a-Chemical, 2003. **204**: p. 473-481.
15. Li, F. and B.C. Gates, *Synthesis and structural characterization of iridium clusters formed inside and outside the pores of zeolite NaY.* Journal of Physical Chemistry B, 2003. **107**(42): p. 11589-11596.
16. Weber, W.A. and B.C. Gates, *Hexarhodium clusters in NaY zeolite: Characteristics by infrared and extended x-ray absorption fine structure spectroscopies.* Journal of Physical Chemistry B, 1997. **101**(49): p. 10423-10434.
17. Kundu, A., Y.G. Shul, and D.H. Kim, *Methanol Reforming Processes*, in *Advances in Fuel Cells*, T.S. Zhao, K.-D. Kreuer, and T. Nguyen, Editors. 2007, Elsevier.
18. Manzoli, M., A. Chiorino, and F. Boccuzzi, *Interface species and effect of hydrogen on their amount in the CO oxidation on Au/ZnO.* Applied Catalysis B-Environmental, 2004. **52**(4): p. 259-266.
19. Liu, S.T., et al., *Hydrogen production by oxidative methanol reforming on Pd/ZnO.* Applied Catalysis a-General, 2005. **283**(1-2): p. 125-135.
20. Chen, G.W., et al., *Methanol oxidation reforming over a ZnO-Cr2O3/CeO2-ZrO2/Al2O3 catalyst in a monolithic reactor.* Catalysis Today, 2007. **125**(1-2): p. 97-102.
21. Semelsberger, T.A., et al., *Generating hydrogen-rich fuel-cell feeds from dimethyl ether (DME) using Cu/Zn supported on various solid-acid substrates.* Applied Catalysis a-General, 2006. **309**(2): p. 210-223.
22. Thomas, J.M., *The ineluctable need for in situ methods of characterising solid catalysts as a prerequisite to engineering active sites.* Chemistry-a European Journal, 1997. **3**(10): p. 1557-1562.
23. Lytle, F.W., *The EXAFS family tree: a personal history of the development of extended X-ray absorption fine structure.* Journal of Synchrotron Radiation, 1999. **6**: p. 123-134.
24. Mosselmans, F. and P. Stephenson. *Extended X-Ray Absorption Fine Structure*. [cited 2008; Available from: http://www.srs.dl.ac.uk/xrs/Theory/theory.html#intro.
25. Rehr, J.J. *Introduction to XAS Theory*. 2003 [cited 2008]; Available from: http://cars9.uchicago.edu/xafs/NSLS_EDCA/July2003/Rehr.pdf.
26. Castano, P., et al., *The role of zeolite acidity in coupled toluene hydrogenation and ring opening in one and two steps.* Industrial & Engineering Chemistry Research, 2008. **47**(3): p. 665-671.
27. Zheng, J., M. Guo, and C. Song, *Characterization of Pd catalysts supported on USY zeolites with different SiO2/Al2O3 for the hydrogenation of naphthalene in the presence of benzothiophene.* Fuel Processing Technology, 2008. **89**(4): p. 467-474.

28. Ivanova, E. and K. Hadjiivanov, *Polycarbonyls of Rh+ formed after interaction of CO with Rh-MFI: an FTIR spectroscopic study.* Physical Chemistry Chemical Physics, 2003. **5**(3): p. 655-661.
29. Ivanova, E., et al., *Unusual carbonyl-nitrosyl complexes of Rh2+ in Rh-ZSM-5: A combined FTIR spectroscopy and computational study.* Journal of Physical Chemistry C, 2007. **111**(28): p. 10412-10418.
30. Ivanova, E., et al., *New type of rhodium gem-dicarbonyls formed in Rh-ZSM-5: An FTIR spectroscopy study.* Journal of Catalysis, 2005. **236**(1): p. 168-171.
31. Vanzon, J.B.A.D., et al., *An Exafs Study of the Structure of the Metal-Support Interface in Highly Dispersed Rh/Al2o3 Catalysts.* Journal of Chemical Physics, 1985. **82**(12): p. 5742-5754.
32. Kirlin, P.S., et al., *Surface Catalytic Sites Prepared from [Hre(Co)5] and [H3re3(Co)12] - Mononuclear, Trinuclear, and Metallic Rhenium Catalysts Supported on Mgo.* Journal of Physical Chemistry, 1990. **94**(22): p. 8439-8450.
33. Vaarkamp, M., J.C. Linders, and D.C. Koningsberger, *A New Method for Parameterization of Phase-Shift and Backscattering Amplitude.* Physica B-Condensed Matter, 1995. **209**(1-4): p. 159-160.
34. *Crystal Structures*. 2 ed, ed. R.W.G. Wycoff. Vol. 1. 1963, New York: John Wiley & Sons.
35. Schaefer, W.P. and R.E. Marsh, *Oxygen-Carrying Cobalt Compounds .I. Bis(Salicylaldehyde)Ethylenediiminecobalt(2) Monochloroformate.* Acta Crystallographica Section B-Structural Crystallography and Crystal Chemistry, 1969. **B 25**: p. 1675-&.
36. Ramaker, D.E., et al., *Understanding atomic x-ray absorption fine structure in x-ray absorption spectra.* Journal of Physics-Condensed Matter, 1998. **10**(39): p. 8753-8770.
37. Ramaker, D.E., X. Qian, and W.E. O'Grady, *'Atomic' X-ray absorption fine structure: a new tool for examining electronic and ionic polarization effects.* Chemical Physics Letters, 1999. **299**(2): p. 221-226.
38. Cook, J.W. and D.E. Sayers, *Criteria for Automatic X-Ray Absorption Fine-Structure Background Removal.* Journal of Applied Physics, 1981. **52**(8): p. 5024-5031.
39. Grunwaldt, J.D., et al., *2D-mapping of the catalyst structure inside a catalytic microreactor at work: Partial oxidation of methane over Rh/Al2O3.* Journal of Physical Chemistry B, 2006. **110**(17): p. 8674-8680.
40. Kohno, Y., et al., *Photoenhanced reduction of CO2 by H-2 over Rh/TiO2 - Characterization of supported Rh species by means of infrared and X-ray absorption spectroscopy.* Journal of Molecular Catalysis a-Chemical, 2001. **175**(1-2): p. 173-178.
41. Nachtigall, P., et al., *FTIR study of CO interactions with Li+ ions in micro- and mesoporous matrices: Coordination and localization of Li+ ions.* Journal of Physical Chemistry C, 2007. **111**(30): p. 11353-11362.

42. Fulton, J.L., et al., *When is a nanoparticle a cluster? An operando EXAFS study of amine borane dehydrocoupling by Rh4-6 clusters.* Journal of the American Chemical Society, 2007. **129**(39): p. 11936-11949.
43. Shido, T., T. Okazaki, and M. Ichikawa, *Exafs and Ftir Characterization of Tetrarhodium Carbonyl Clusters Attached on Tris-(Hydroxymethyl)Phosphine Grafted Silica Catalytically Active for Olefin Hydroformylation.* Catalysis Letters, 1993. **20**(1-2): p. 37-48.
44. Grunwaldt, J.D., L. Basini, and B.S. Clausen, *In situ EXAFS study of Rh/Al2O3 catalysts for catalytic partial oxidation of methane.* Journal of Catalysis, 2001. **200**(2): p. 321-329.

## Appendix

The following are Fourier Transform and chi plots of all EXAFS data for the thermally treated catalysts.

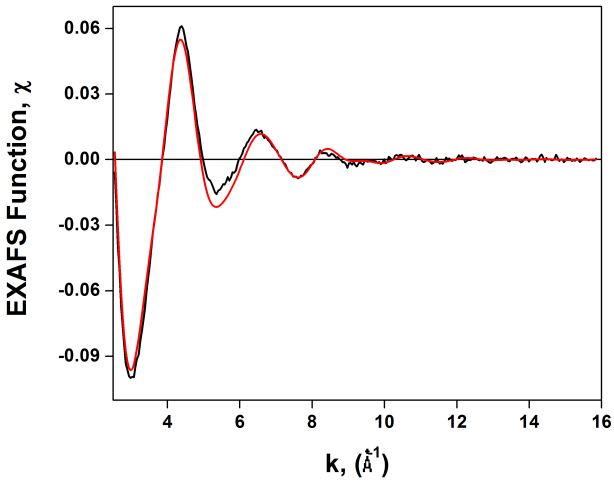


**Figure A.1. The chi plot of catalyst Si/Al 23:Rh(I), showing the fit of the model (red) versus the experimental data (black).**

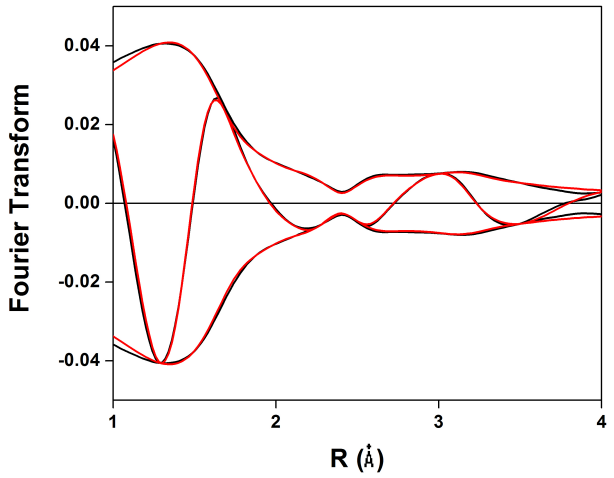


**Figure A.2 The Fourier Transform plot of catalyst Si/Al 23:Rh(I), showing the fit of the model (red) versus the experimental data (black).**

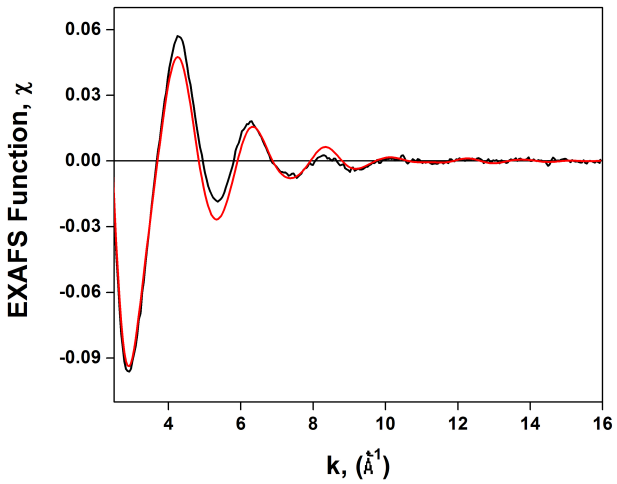


**Figure A.3. The chi plot of catalyst Si/Al 50:Rh(I), showing the fit of the model (red) versus the experimental data (black).**

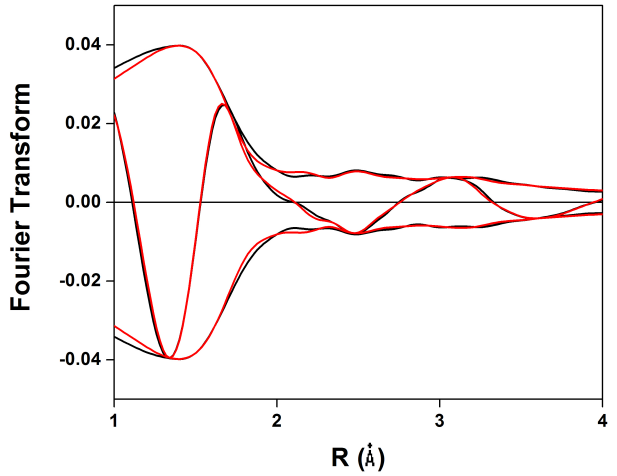


**Figure A.4. The Fourier Transform plot of catalyst Si/Al 50:Rh(I), showing the fit of the model (red) versus the experimental data (black).**

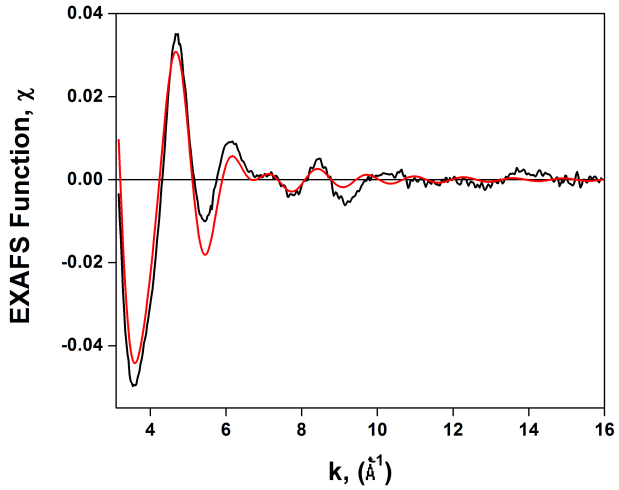


**Figure A.5. The chi plot of catalyst Si/Al 280:Rh(I), showing the fit of the model (red) versus the experimental data (black).**

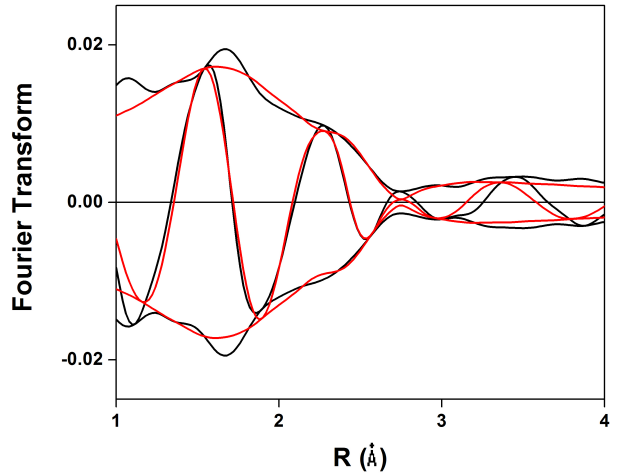


**Figure A.6. The Fourier Transform plot of catalyst Si/Al 280:Rh(I), showing the fit of the model (red) versus the experimental data (black).**

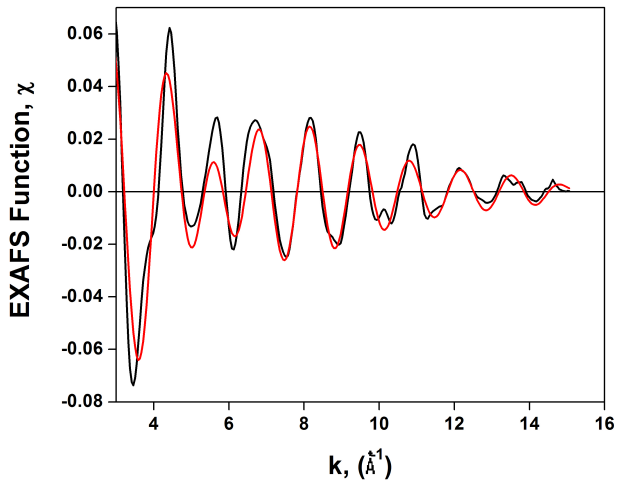


**Figure A.7. The chi plot of catalyst Si/Al 50:Rh(II), showing the fit of the model (red) versus the experimental data (black).**

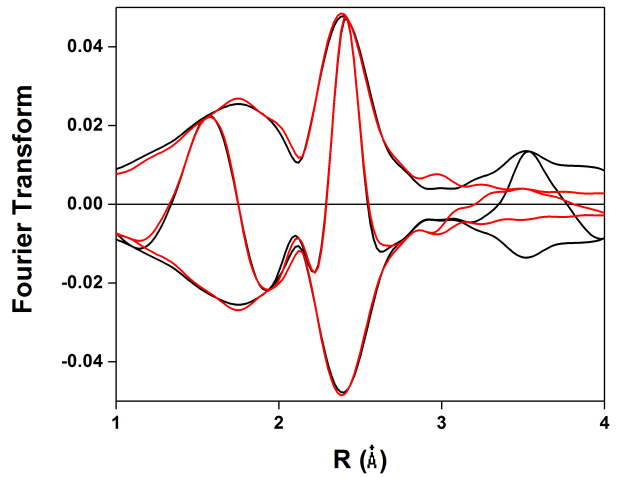


**Figure A.8. The Fourier Transform plot of catalyst Si/Al 50:Rh(II), showing the fit of the model (red) versus the experimental data (black).**

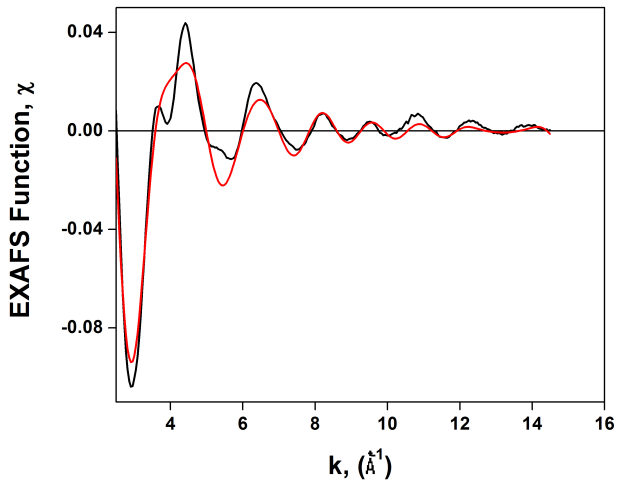


**Figure A.9. The chi plot of catalyst Si/Al 280:Rh(II), showing the fit of the model (red) versus the experimental data (black).**

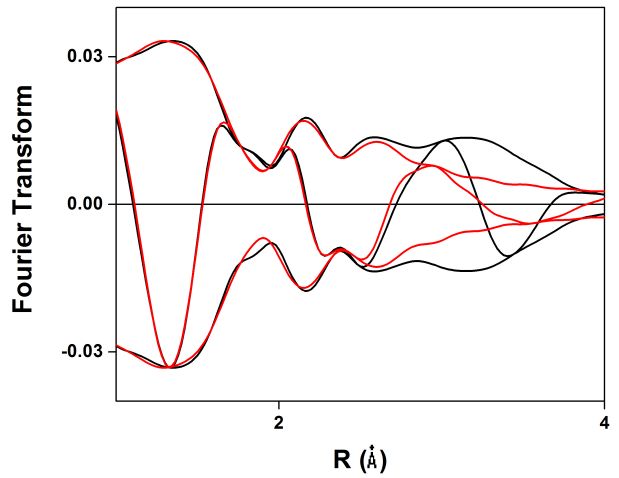


**Figure A.10. The Fourier Transform plot of catalyst Si/Al 280:Rh(II), showing the fit of the model (red) versus the experimental data (black).**